Drug Design, Development and Therapy

Dovepress
Taylor & Francis Group

Open Access Full Text Article

ORIGINAL RESEARCH

Oleanolic Acid@SPIONs Alleviates Lipid-Oxidative Stress Injury of Zebrafish Blood Vessels via Regulating the Expression of JNK and MAPK Signaling Pathways in Vascular Endothelial Cells

Hongguo Gao[1,2,*], Te Liu[3,*], Junfeng Liu[4,*], Lian Yang[3,*], Luxi Liu[5,*], Zeyu Cui[3], Xiling Du[6], Yun Gu[1–3], Peirong Huang[7–9]

[1]Department of Traditional Chinese Medicine, Graduate School, Jiangxi University of Traditional Chinese Medicine, Nanchang, 330100, People's Republic of China; [2]Department of Geriatric Medicine, Longhua Hospital, Shanghai University of Traditional Chinese Medicine, Shanghai, 200031, People's Republic of China; [3]Shanghai Geriatric Institute of Chinese Medicine, Shanghai University of Traditional Chinese Medicine, Shanghai, 200031, People's Republic of China; [4]Department of Nephrology, Shanghai Quyang Hospital, Shanghai, 200083, People's Republic of China; [5]Class 1, Grade 8, Shanghai Wenlai Middle School, Shanghai, 201101, People's Republic of China; [6]School of Life Science and Technology, Tongji University, Shanghai, 200092, People's Republic of China; [7]Department of Ophthalmology, Shanghai General Hospital, Shanghai Jiao Tong University School of Medicine, Shanghai, 200080, People's Republic of China; [8]National Clinical Research Center for Eye Diseases, Shanghai, 200080, People's Republic of China; [9]Shanghai Key Laboratory of Ocular Fundus Diseases, Shanghai, 200080, People's Republic of China

*These authors contributed equally to this work

Correspondence: Peirong Huang, Department of Ophthalmology, Shanghai General Hospital, Shanghai Jiao Tong University School of Medicine, 100 haining Road, Hongkou District, Shanghai, 200031, People's Republic of China, Tel +86-21-63240090, Email peirong_huang@126.com; Yun Gu, Department of Traditional Chinese Medicine, Graduate School, Jiangxi University of Traditional Chinese Medicine, 1688 Meiling Avenue, Zhaoxian Town, Xinjian District, Nanchang, 330100, People's Republic of China, Tel +86-791-87119529, Email birgitgu@163.com

Background and Aims: The incidence of and mortality due to atherosclerosis, a leading cause of cardiovascular disease, is rising annually. Oleanolic acid (OA), an active component of the traditional Chinese medicine Ligustrum lucidum, has been proven to have significant anti-inflammatory and lipid-lowering potential.

Methods: The fli1a::EGFP+ zebrafish fed with oxidized low-density lipoprotein (oxLDL) diet were used as Atherosclerosis model. The zebrafish Atherosclerosis model were fed with oxalic acid driven by superparamagnetic ferrite nanoparticles (OA@SPIONs). Isolation and enrichment of fli1a::EGFP+ zebrafish endothelial cells (zeECs) from each group and RNA-seq to analyze changes in gene transcription. The H&E, MASSION, Oil red O staining were used to identifying pathological phenotypes.

Results: Pathological staining and ultrastructural identification indicated that oxLDL-treated zebrafish exhibited significant lipid plaque deposition and signs of cellular senescence that were significantly alleviated by OA@SPIONs treatment. OA@SPIONs treatment notably improved the ultrastructural integrity of myocardial, liver, and intestinal tissues in oxLDL-treated zebrafish. The RNA-seq results showed that OA@SPIONs treatment significantly altered the expression levels of multiple gene transcripts in zeECs. The KEGG analysis revealed that in the OA@SPION-treated group zeECs, key genes in the JNK and MAPK signaling pathways, such as Cacna1c, Rab1ab (Ras), Map3k1 (MEKK1), Mapk8b (JNK), and JunD, had significantly lower sequencing signals than in the oxLDL+SPION-treated group zeECs. The qPCR results were highly consistent with the RNA-sequencing data.

Conclusion: Therefore, our results confirm that SPIONs can effectively deliver OA for stable release in zebrafish and provide strong evidence that OA@SPION-polyethyleneimine exerts protective effects against oxLDL-induced damage in zebrafish by downregulating the expression of the JNK and MAPK signaling pathways.

Keywords: atherosclerosis, super paramagnetic iron oxide nanoparticles (SPIONs), zebrafish, oleanolic acid (OA), JNK and MAPK signaling pathways

Received: 14 January 2025
Accepted: 10 April 2025
Published: 15 April 2025

Introduction

Atherosclerosis is a major cause of cardiovascular disease development. With changes in modern diet and lifestyle, the incidence and mortality rate of atherosclerosis have been increasing annually.[1–5] Blood vessels are widely distributed throughout various tissues and organs in the body. Atherosclerosis is characterized by lipid deposition in the arterial walls and chronic inflammation. Oxidized low-density lipoprotein (oxLDL) stimulates vascular endothelial cells (ECs) to secrete large amounts of inflammatory mediators, driving the infiltration of inflammatory cells beneath the ECs.[5–7] This process leads to chronic inflammation, ultimately forming atherosclerotic plaques.[1–3,8] It is now believed that vascular aging is a significant factor in many age-related diseases and individual aging.

The main physiological functions of ECs include acting as barriers, secreting factors, and participating in angiogenesis.[3,9] Research has shown that modified lipoproteins, particularly oxLDL, can induce EC apoptosis and trigger atherosclerosis, making them early risk factors for atherosclerosis.[10] Chronic and prolonged endoplasmic reticulum stress can induce the unfolded protein response, leading to EC dysfunction, which results in cell apoptosis, inflammation, and atherosclerosis.[11] Triglyceride-rich lipoproteins, which are produced in patients with hypertriglyceridemia, can induce high expression of VCAM-1 in aortic ECs, ultimately leading to atherosclerosis.[11] Additionally, EC aging significantly affects processes such as angiogenesis, heart failure, and atherosclerosis, while the clearance of senescent cells can effectively inhibit the progression of related pathologies.[12–14] Thus, ECs play a crucial role in the development of atherosclerosis.

Oleanolic acid (OA) is a pentacyclic triterpenoid compound isolated and extracted from the whole herb of *Swertia mileensis* of the Gentianaceae family or the fruits of *Ligustrum lucidum*. Existing in both free bodies and ligands,[15,16] OA is widely present in plants, with typical concentrations ranging from 0.2 to 2% and high levels found in the fruits of *Cucurbitaceae* plants and *Ligustrum lucidum*. OA is a broad-spectrum antibacterial agent clinically used to protect liver function, and some studies have also indicated its efficacy in treating bronchitis, acute gastroenteritis, urinary system infections, and cancer.[17,18] Recent research has discovered that OA can enhance cholesterol reverse transport and promote the breakdown and metabolism of cholesterol in the liver. Additionally, OA has been found able to clear lipid deposits from the inner walls of blood vessels.[19,20] These studies provide an intriguing basis for the treatment of atherosclerosis by OA.

Superparamagnetic iron oxide nanoparticles (SPIONs) are nanospheres approximately 20 nm in size.[21–24] Increasing research has shown that by chemically modifying the surface of SPIONs, their hydrophobic properties can be converted into hydrophilic properties, allowing them to effectively disperse in physiological saline or phosphate-buffered saline (PBS) buffer solutions.[21–24] Based on this characteristic and after their surface modification with proteins, liposomes, or polymers, SPIONs have been widely applied in drug delivery and release, magnetic resonance imaging (MRI), tumor magnetic hyperthermia, magnetic chromatography, magnetic transfection, and biosensors.[25,26] Based on these findings, this study aimed to develop a nanodrug delivery system by loading OA onto SPIONs (OA@SPIONs) and explore its therapeutic effects and potential drug targets in an oxLDL-induced atherosclerosis zebrafish model.

Materials and Methods

Preparation of SPIONs Bound Oleanolic Acid

The products of SPIONs (SPION-polyethyleneimine [PEI]) were purchased from NOVOBIO Biotechnology Co., Ltd. (Shanghai, China). In brief, 100 mg of OA (Yuanye Biotechnology, Shanghai, China) in 1.0 mL of phosphate buffer (0.2 mol/L Na_2HPO_4, 0.2 mol/L NaH_2PO_4, pH 6.0) and 100 mg of SPIONs were mixed and then ultrasonicated for 60 min. After the product was separated from the mixture using a neodymium magnet, the product was washed with water and ethanol three times and vacuum-dried at room temperature.

Zebrafish Feeding and Drug Treatment

A total of 300 zebrafish embryos of the transgenic zebrafish line Tg(fli1a::EGFP) were obtained 24 h post-fertilization from the Shanghai Research Centre for Model Organisms (Shanghai, China). All embryos were cultured in E3 zebrafish culture medium (0.58 g/l NaCl, 0.27 g/l KCl, 0.97 g/l CaCl2·2H2O, 0.16 g/l MgCl2·6H2O, 1% methylene blue; pH 7.2;

all from Sigma-Aldrich, St. Louis, MO, USA; Merck KGaA, Darmstadt, Germany) in a fish tank.[27,28] All zebrafish were randomly divided into three groups of 100 dechorionated embryos per group at 48 h post-fertilization (hpf). The WT group was raised under normal conditions without any treatment. The OA@SPIONs-treated group consisted of zebrafish raised in E3 zebrafish culture medium containing 500 μg/mL oxLDL (Yuanye Biotechnology) and 0.2 mg/mL OA@SPIONs.[29,30] The control-treated group consisted of zebrafish raised in E3 zebrafish culture medium containing 500 μg/mL oxLDL (Yuanye Biotechnology) and an equal amount of saline.[31–34] All zebrafish in all groups were raised for 72 h.

Fli1a::EGFP+ Zebrafish Endothelial Cell Isolation And Enrichment

Fli1a::EGFP+zebrafish endothelial cell (zeEC) isolation and enrichment consisted of the following steps. First, 20 mL of 0.25% trypsin (Sigma-Aldrich) was added to a 50 mL centrifuge tube and a 100 fli1a::EGFP zebrafish placed in each tube for incubation in the centrifuge tubes at 28°C with rotation for 6 h. The liquid was mixed by pipetting once every hour. After digestion was complete, the cell was passed by suspension through a 20 mL syringe with a 0.8 mm needle six times. Then, the cell suspension was filtered through a 100 μm cell strainer (BD Falcon, Franklin Lakes, NJ, USA). The cell suspension was collected and centrifuged at 4°C and 1500 rpm for 10 min before the supernatant was removed and the cell pellet resuspended in saline containing 10% fetal bovine serum (Sigma-Aldrich). Next, a zebrafish cell suspension was prepared at 1×10^{10} cells/mL before 0.5 mL of ice-cold sterile PBS (HyClone, Logan, UT, USA) was added, and then a flow cytometer (BD FACS Aria, BD Bioscience, Franklin Lakes, NJ, USA) was used to sort and enrich enhanced green fluorescent protein positive (EGFP+) zeECs.

Transmission Electron Microscopy Analysis

Briefly, tissue samples were fixed with 1% glutaraldehyde (Sigma-Aldrich) for 4 h, followed by fixation with 1% osmium tetroxide for 1 h. The samples were then dehydrated with acetone and embedded in Resin 12 (Ted Pella, Redding, CA, USA). Ultrathin sections (70 nm in thickness) were mounted on copper grids, stained with 1% uranyl acetate (Sigma-Aldrich) and 1% lead citrate (Sigma-Aldrich), and observed and photographed using a JEM-1230 transmission electron microscope (JEOL, Kanagawa, Japan).

Nanoparticle Tracking Analysis

A dark field microscope (NS500; Nanosight, Amesbury, UK) with a 45 mW 405 nm laser and an electron multiplying charge-coupled device (EMCCD) was used to determine the SPIONs by tracking the Brownian motion of single particles.

Hematoxylin and Eosin Staining

In brief, tissue samples were fixed with 4% paraformaldehyde, dehydrated, and embedded in paraffin. Sections with a thickness of 4 μm were cut using a microtome and mounted on slides before being dewaxed using xylene and subjected to a gradient of ethanol dehydration. The samples were stained with hematoxylin at room temperature for 5 min, differentiated with 1% hydrochloric acid ethanol for 30s, and returned to blue with dilute ammonia water for 1 min, followed by rinsing with distilled water for 5 min. Subsequently, the samples were stained with eosin at room temperature for 2 min and rinsed with distilled water for 2 min. A gradient of ethanol was used for dehydration. The samples were cleared with xylene for 2 min before being mounted with neutral gum.

Masson Staining

Masson staining was performed according to the instructions of the Masson staining kit (Beyotime Biotechnology, Jiangsu, China). After embedding, sectioning, and dewaxing the tissue samples, they were stained with the prepared hematoxylin solution (A1 and A2 mixed at a 1:1 ratio) for 10 min, followed by differentiation in acidic ethanol for 5s and rinsing with distilled water for 10s. The Masson blue solution was applied to the samples for 3 min, followed by rinsing of the samples with distilled water for 1 min. The samples were then stained with Lichun red solution for 7 min, washed with weak acid working solution for 1 min, rinsed with phosphomolybdic acid solution for 1 min, and again washed with

weak acid working solution for 1 min. The aniline blue solution was used for staining of the samples for 2 min, followed by washing with weak acid working solution for 1 min. Subsequently, rapid dehydration was performed with 95% ethanol, followed by three rounds of dehydration with anhydrous ethanol for 10s each. Finally, the samples were cleared with xylene three times for 2 min each before they were mounted with neutral gum for observation and photography under a microscope.

Oil Red O Staining

To perform Oil Red O staining, an adequate number of zebrafish were collected, rinsed with PBS, and fixed with 4% paraformaldehyde (PFA) at room temperature for 1 h or overnight at 4°C. After treatment with 25, 50, 75, and 100% propylene glycol diluted with PBS, the samples were stained with Oil Red O solution overnight in the dark at room temperature. Subsequently, the samples were treated sequentially with 75, 50, and 25% propylene glycol diluted with PBS and preserved in glycerol before photographs were taken under a microscope.

Senescence-Associated β-Galactosidase Staining

SA-β-gal staining was performed according to the instructions of the SA-β-gal staining kit (Beyotime). In brief, the samples were rinsed once with PBS and then fixed with the fixing solution for 10 to 15 min. After the samples were washed twice with PBS, 800 μL of freshly prepared staining solution, in which 1 mL included 930 μL of staining solution, 10 μL of solution A, 10 μL of solution B, and 50 μL of X-gal (20 mg/mL), was added. The samples were then incubated in a 37°C incubator in the dark for 16 h. After staining, the samples were washed twice with PBS before being observed and photographed under a microscope.

Filipin Staining

To perform filipin staining, the samples were rinsed twice with PBS and fixed at room temperature with 4% PFA for 30 min. In a dark environment, filipin staining solution, of which the storage solution is a 25 mg/mL dimethyl sulfoxide (DMSO) solution and the working solution is a 50 μg/mL (DMSO) solution (Yuanye Biotechnology, Shanghai, China), was added to stain the samples for 1 h. After staining, the samples were washed several times with PBS, mounted with an aqueous mounting medium, and observed and photographed under a fluorescence microscope.

RNA-Sequencing

In brief, the total RNA from each group of samples was assessed for integrity using agarose gel electrophoresis and quantified with a NanoDrop ND-1000 (Thermo Fisher Scientific) for further quality control. For sequencing library construction, 1 to 2 μg of total RNA from each sample was selected. Total RNA was first enriched for mRNA using the NEB Next® Poly(A) mRNA Magnetic Isolation Module (New England BioLabs, Southwick, MA, USA) or treated with the RiboZero Magnetic Gold Kit (Illumina, San Diego, CA, USA) for rRNA removal. The RNA products after treatment were used to construct libraries with the KAPA Stranded RNA-Seq Library Prep Kit (Illumina). The constructed libraries underwent quality control (QC) using the Agilent 2100 Bioanalyzer (Agilent Technologies, Santa Clara, CA, USA), assessing library concentration, fragment size of 400 to 600 bp, and the presence of adapters and other factors, and further quantified using quantitative polymerase chain reaction (qPCR; Shanghai Personal Biotechnology Co., Ltd., Shanghai, China). Based on the quantification results and the final sequencing data requirements, the sequencing libraries from different samples were mixed, and the sequencing process was entered. The sequencing data generated by the Illumina NovaSeq 6000 (Illumina) were raw sequencing data that had undergone QC to evaluate whether the sequencing data could be used for subsequent data analysis.

After QC, the trimmed data produced through the preprocessing and filtering steps, during which adapter sequences and overly short fragments were removed, was aligned to the reference genome. Statistical analysis of the alignment results, which included determination of the alignment rate, ribosomal RNA (rRNA)/mitochondrial RNA (mtRNA) content, and potential bias of sequencing fragments on genes, was performed to determine whether the alignment results could be used for further data analysis. If the alignment results were satisfactory, a series of analyses were conducted, including gene and transcript expression quantification, various analyses based on gene expression levels, differential

gene expression screening, gene ontology (GO) functional enrichment analysis, and pathway significance enrichment analysis. Finally, various visualization views, such as scatter plots, volcano plots, and clustering diagrams, were generated to facilitate data browsing (Shanghai Personal Biotechnology Co., Ltd).

RNA Extraction, Reverse Transcription, and Quantitative Real-Time PCR

According to the RNAprep Pure Tissue Kit (TIANGEN Biotech (Beijing) Co., Ltd., Beijing, China) instructions, cells were mixed with 800 μL of lysis buffer and vigorously shaken. Next, 200 μL of chloroform was added, and the mixture was inverted and mixed well. The sample was then centrifuged at 4°C at 13,400 ×*g* for 15 min, and the supernatant was collected. After two volumes of anhydrous ethanol relative to the supernatant volume were added and mixed well, the mixture was centrifuged at 4°C at 13,400 ×*g* for 30 min. The RNA pellet was resuspended in 500 μL of 75% ethanol and centrifuged at 4°C at 13,400 ×*g* for 5 min. The excess liquid was removed, and the pellet was dissolved in 300 μL of diethyl pyrocarbonate (DEPC)-treated water. One microliter of the RNA solution was used to measure the OD260/OD280 ratio (generally controlled between 1.8 and 2.0) to determine RNA purity and total concentration.

Following the instructions of the messenger RNA (mRNA) first-strand complementary DNA (cDNA) synthesis kit (TIANGEN Biotech), 20 μL of total RNA (100 ng/μL), 25 μL of 2 × mRNA RT Reaction Buffer, 4 μL of 1 × mRNA RT Enzyme Mix, and 6 μL of RNase-Free deionized water were mixed thoroughly. The following reactions were conducted in a PCR machine: the sample was incubated at 42°C for 60 min for poly(A) tail addition and reverse transcription before being incubated at 95°C for 3 min for enzyme inactivation. Subsequently, following the instructions of the mRNA qPCR Detection Kit (TIANGEN Biotech), the following reagents and samples were added according to the system: 10 μL of 2 × mRcute Plus mRNA Premix (with SYBR), 1 μL each of 1 × Forward Primer and Reverse Primer (10 μM), 4 μL of first-strand cDNA, and 4 μL of deionized water. The following reactions were performed on the real-time fluorescence quantitative PCR instrument: 95°C for 15 min, 94°C for 20s, and 60°C for 34s while reading fluorescence values for a total of 40 cycles. The relative expression levels of genes were determined using the 2-ΔΔCt method, where ΔCt = Ct_genes – Ct_18s rRNA; ΔΔCt = ΔCt_all_groups – ΔCt_control_group. The mRNA expression levels were normalized according to the expression level of 18s rRNA.

Statistical Analysis

Each experiment was performed at least three times, and the data are shown as the mean (standard error) where applicable. Differences were evaluated using the Student's *t* test, and a *P* value less than 0.05 was considered statistically significant. Meanwhile, Using the One-Way ANOVA with Bonferroni test for multiple group comparisons, significant interactions, differences and main effects for all statistical tests were analyzed (α = 0.05). A P value less than 0.05 was considered to be statistically significant.

Results

The Successful Loading of OA@SPION-PEI Has the Advantages of Good Dispersibility, Stability, and Non-Toxicity

In order to overcome the disadvantages of poor solubility and stability of OA and improve the therapeutic effect, using a distributed synthesis method, we loaded polyethyleneimine (PEI) onto the surface of SPIONs and then incorporated OA to form an OA@SPION-PEI nanocomposite (Figure 1A). The SEM and TEM results indicated that OA@SPION-PEI exhibited a spherical shape, with a diameter of approximately 50 nm (Figure 1B and C). NAT analysis confirmed that the particle size of OA@SPION-PEI ranged from 28 to 149 nm (Figure 1D).

The results of Fourier transform infrared spectroscopy (FTIR) shown that the vibration peak of OA was at 1000–1500 nm, and the simultaneous presence of this peak in the curve of the OA@SPION-PEI confirmed the successful loading of OA onto SPION in the nanomedicine (Figure 1E). The results of UV spectrophotometer detection indicated that the absorption peak of OA was mainly concentrated around 260 nm, while the ultraviolet absorption peak of SPION was mainly located around 400–550 nm; Therefore, the absorption peaks of OA@SPION-PEI were mainly located between 250–300 nm and 400–550 nm (Figure 1F). The Zeta potential detection results revealed that both SPION and OA had

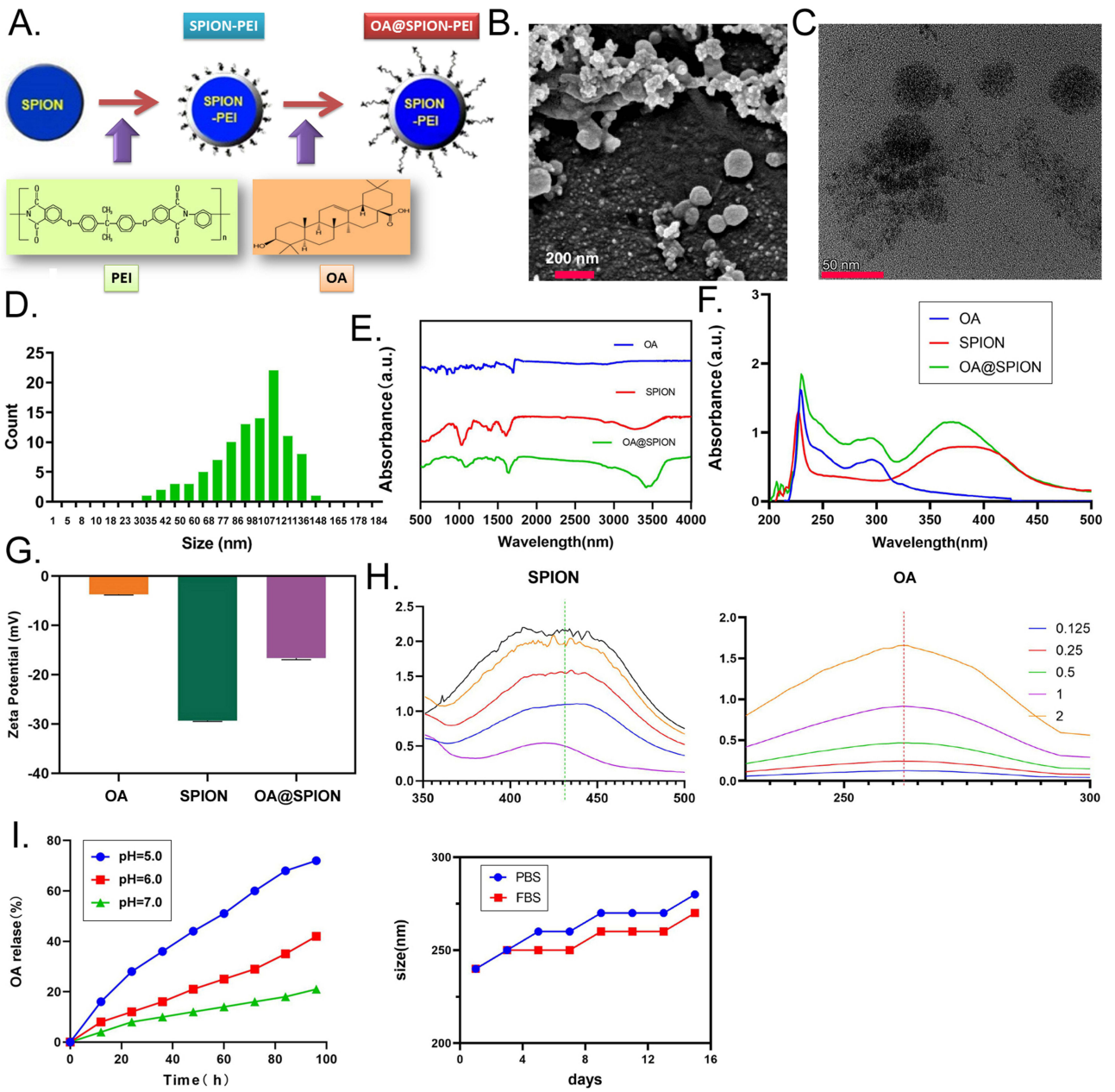

Figure 1 The successful loading of OA@SPION-PEI has the advantages of good dispersibility and stability. (**A**) Loading process of OA and SPION-PEI. (**B**) Scanning electron microscopy results showed that surface of OA@SPION-PEI was a spherical structure. (**C**) Transmission electron microscopy results showed that OA@SPION-PEI appeared spherical with a diameter of approximately 50 nm. Scale bar = 50 nm. (**D**) NAT detection results confirmed that the particle size of OA@SPION-PEI was between 28 and 149 nm. (**E**) The results of Fourier transform infrared spectroscopy (FTIR) assay. (**F**) The results of UV spectrophotometer detection. (**G**) The Zeta potential detection results revealed that the zeta potential of OA@SPION-PEI was approximately −16.63±0.31 mV. (**H**) The UV visible spectrophotometer detection results showed that the packaging closure rate of OA in nanomedicine was greater than 60%. (**I**) The in vitro release rate of OA in OA@SPION-PEI was detected in different pH environments.

negative and relatively stable Zeta potentials; Meanwhile, The zeta potential of OA@SPION-PEI was approximately −16.63±0.31 mV (Figure 1G). In addition, the UV visible spectrophotometer detection results showed that the packaging closure rate of OA in nanomedicine was greater than 60% (Figure 1H).

In order to evaluate the controlled release ability of the nano drug delivery system, the in vitro release rate of OA in OA@SPION-PEI was detected in different pH environments. The experimental results showed that the pH=5.0 environment is more likely to stimulate the release of OA than the pH=7.0 environment (Figure 1I). Under acidic conditions, the release rate of OA significantly increases, making it easier to exert anti-tumor effects. In addition, the

experimental results also showed that with the increase of time, the diameter of OA@SPION-PEI exposed to serum (FBS) was significantly smaller than that exposed to PBS. The experimental results indicated that OA@SPION-PEI in serum was not prone to aggregation. The results of the above experiments indicated that the loading of OA@SPION-PEI nanomedicine is successful, and it has good dispersibility and stability characteristics.

To assess whether OA@SPION-PEI has any toxic effects on zebrafish growth and development, we added 21 mg/mL of OA@SPION-PEI to zebrafish embryos 0 days post-fertilization (dpf) and maintained continuous culture until 3 dpf. Microscopic examination revealed that the zebrafish embryos developed normally without any morphological defects in their organs. All zebrafish successfully progressed to the juvenile stage, with clear green fluorescence observed in the vascular regions (Figure 2). The experimental results indicate that OA@SPION-PEI has no toxic side effects on zebrafish growth and development.

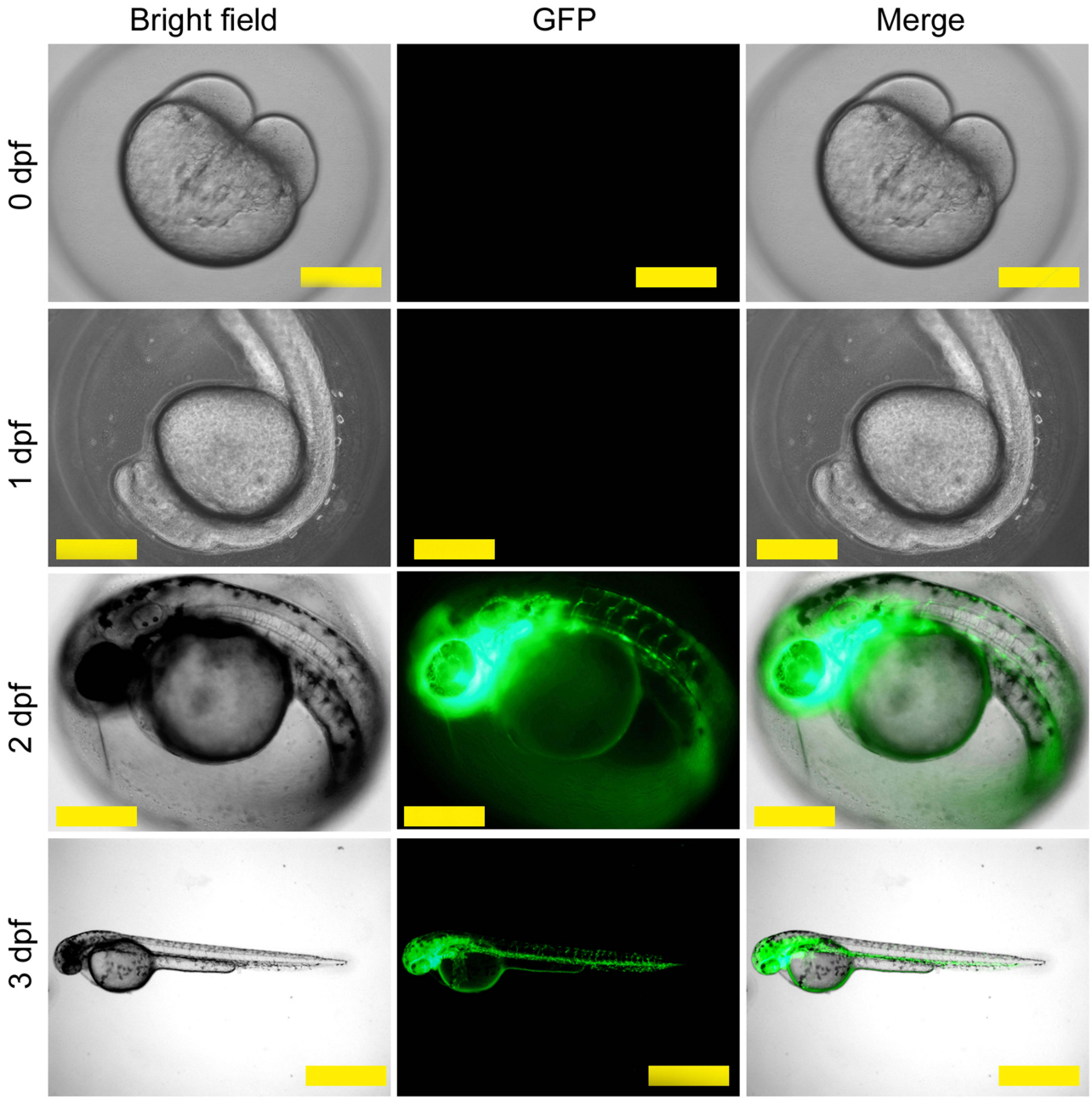

Figure 2 OA@SPION-PEI has no effect on zebrafish growth and development. Observation of zebrafish embryonic development under microscopy. Scale bar: 500 μm.

https://doi.org/10.2147/DDDT.S512752

OA@SPION-PEI Significantly Alleviates Lipid Deposition and Organ Pathological Aging Induced by oxLDL in Zebrafish

H&E staining revealed that the zebrafish in the oxLDL+SPIONs group exhibited vacuolar structures in multiple organs and notable muscle damage, including myocardial injury, suggesting lipid deposition as the likely cause. However, the zebrafish in the oxLDL+OA@SPION-treated group showed significant restoration of organ morphology (Figure 3A). Masson's staining indicated that although both the oxLDL+SPIONs and oxLDL+OA@SPION-treated groups exhibited pronounced deep red staining in various tissues, especially in muscle, indicating significant lipid deposition, the organ morphology of the oxLDL+OA@SPION-treated group appeared more intact (Figure 3B). SA-β-gal staining revealed that although all three groups exhibited positive staining, the oxLDL+SPIONs group displayed a dark green color, particularly in the yolk sac region, indicating a higher degree of organ aging. In contrast, the oxLDL+OA@SPION-treated group demonstrated significantly reduced SA-β-gal staining, suggesting marked improvement in organ aging (Figure 3C).

Additionally, Oil Red O staining indicated that the oxLDL+SPIONs group exhibited pronounced deep red staining, particularly in the yolk sac region, reflecting high levels of organ lipid deposition. In contrast, the oxLDL+OA@SPION-treated group displayed a lighter red color, indicating significant improvement in lipid deposition (Figure 4A). The results of filipin staining were consistent with those of Oil Red O staining (Figure 4B). Furthermore, TEM examination revealed significant improvements in the ultrastructural integrity of myocardial, hepatic, and intestinal tissues in the oxLDL +OA@SPION-treated group (Figure 5). The results of these multiple pathological assessments suggest that OA@SPION can significantly alleviate lipid deposition and pathological organ aging induced by oxLDL in zebrafish.

oxLDL Alters the Expression Levels of Multiple Gene Transcripts in zeECs

Using flow cytometry sorting technology, GFP+ zeECs were enriched from the somatic cells of zebrafish, and RNA seq was utilized to identify differences in gene transcript levels among the three sample groups. A total of 25,432 gene transcripts were detected across the three samples (Figure 6A and Supplementary Data Figure S1). Bidirectional clustering analysis was performed on the intersection of differentially expressed genes across all comparison groups using the R language packages pheatmap and ComplexHeatmap. Based on the expression levels of the same gene in different samples and the expression patterns of different genes within the same sample, the transcripts were classified into nine clusters (Figure 6A and Supplementary Data Figure S1). Specifically, gene sets in Clusters 1, 3, and 4 exhibited significantly higher expression levels in the untreated group (WT) and the oxLDL+OA@SPION treated group (T) compared with the oxLDL+SPIONs group (M; Figure 6B and Supplementary Data Figure S2). Conversely, gene sets in Clusters 7, 8, and 9 displayed opposite expression trends (Figure 6B and Supplementary Data Figure S2). All transcripts corresponded to genes located on 25 chromosomes (Figure 6C and Supplementary Data Figure S3). Using the criteria of log2FoldChange > 2 for significantly upregulated genes and log2FoldChange < -2 for significantly downregulated genes, all transcripts were filtered. The statistical results indicated that in the comparison of the oxLDL+SPIONs group vs the untreated group, there were 484 significantly upregulated gene transcripts and 294 significantly downregulated gene transcripts, and in the comparison of the oxLDL+OA@SPION treated group vs the oxLDL+SPIONs group, there were 486 significantly upregulated gene transcripts and 203 significantly downregulated gene transcripts (Figure 6D). Among these, 43 gene transcripts were identified in the intersection of significantly differentially expressed genes across the three groups (Figure 6E).

GO analysis of the significantly differentially expressed gene transcripts revealed that in the comparison of the oxLDL +SPIONs and untreated groups, the differentially expressed gene transcripts were mainly associated with biological processes (BPs) such as the response to xenobiotic stimuli and molecular functions (MFs), eg, peptidase activity. In the comparison of the oxLDL+OA@SPION-treated and oxLDL+SPIONs groups, the differentially expressed gene transcripts were primarily related to intracellular sequestering of the iron ion, a BP; lactose synthase activity, an MF; and apolipoprotein B mRNA editing enzyme complex, a cellular component (CC; Figure 6F and Supplementary Data Figure S4). Furthermore, Kyoto Encyclopedia of Genes and Genomes (KEGG) analysis revealed that the differentially expressed gene transcripts in the comparison of the oxLDL+SPIONs and untreated groups were mainly involved in signaling pathways such as the Toll-like receptor signaling pathway. In the comparison of the oxLDL+OA@SPION-treated and

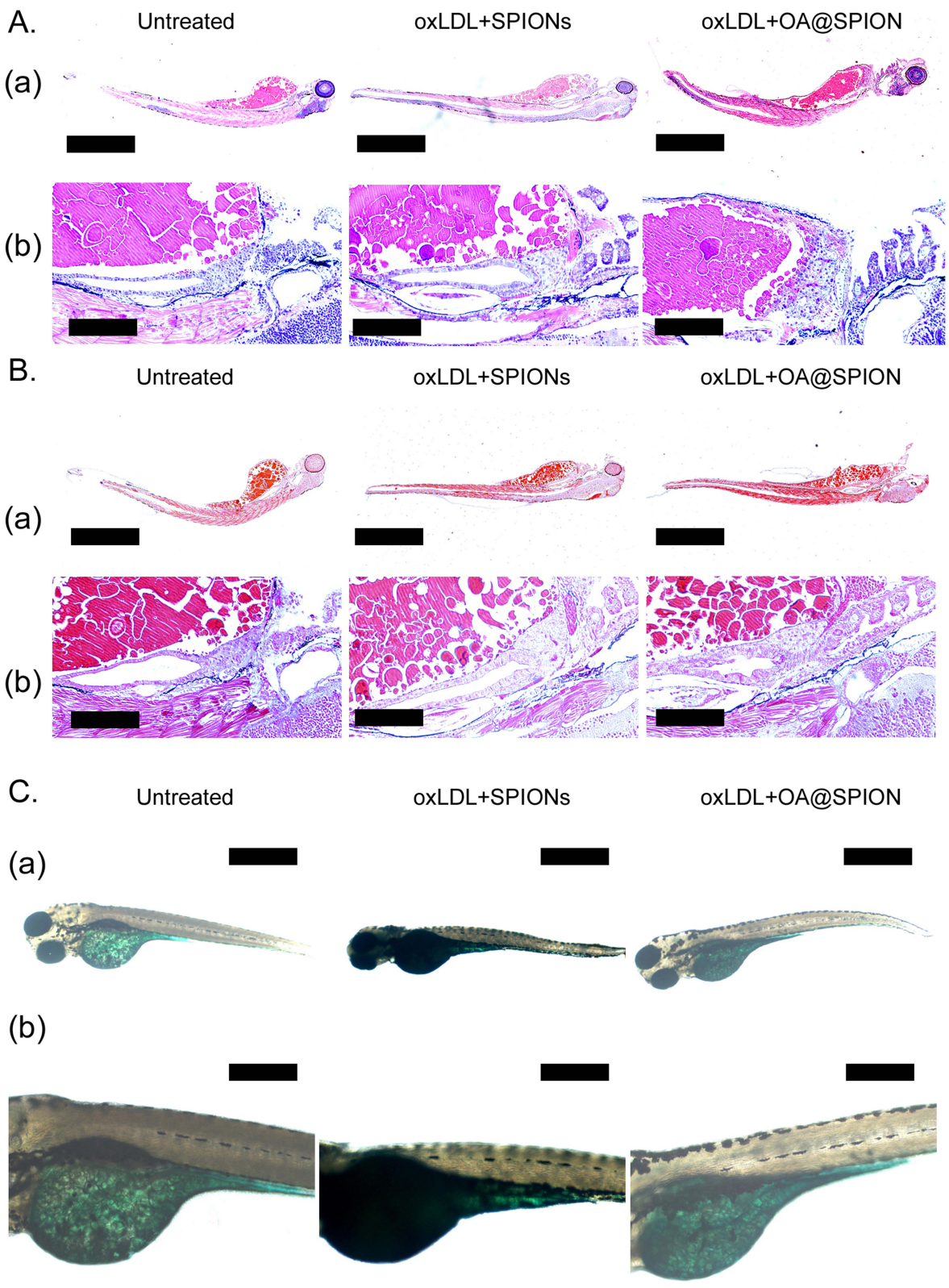

Figure 3 Pathological staining shows that OA@SPION-PEI alleviates oxLDL-induced organ damage and pathological aging in zebrafish. (**A**) H&E staining results showed significant restoration of morphology in various organs of zebrafish treated with OA@SPION-PEI. (a) Magnification: 40×. Scale bar: 500 μm. (b) Magnification: 200×. Scale bar: 100 μm. (**B**) Masson staining results indicated that OA@SPION-PEI significantly restored the structural integrity of zebrafish tissues and organs. (a) Magnification: 40×. Scale bar: 500 μm. (b) Magnification: 200×. Scale bar: 100 μm. (**C**) SA-β-gal staining resules demonstrated that OA@SPION-PEI significantly improved the degree of organ aging in zebrafish. (a) Magnification: 40×. Scale bar: 500 μm. (b) Magnification: 200×. Scale bar: 500 μm.

https://doi.org/10.2147/DDDT.S512752

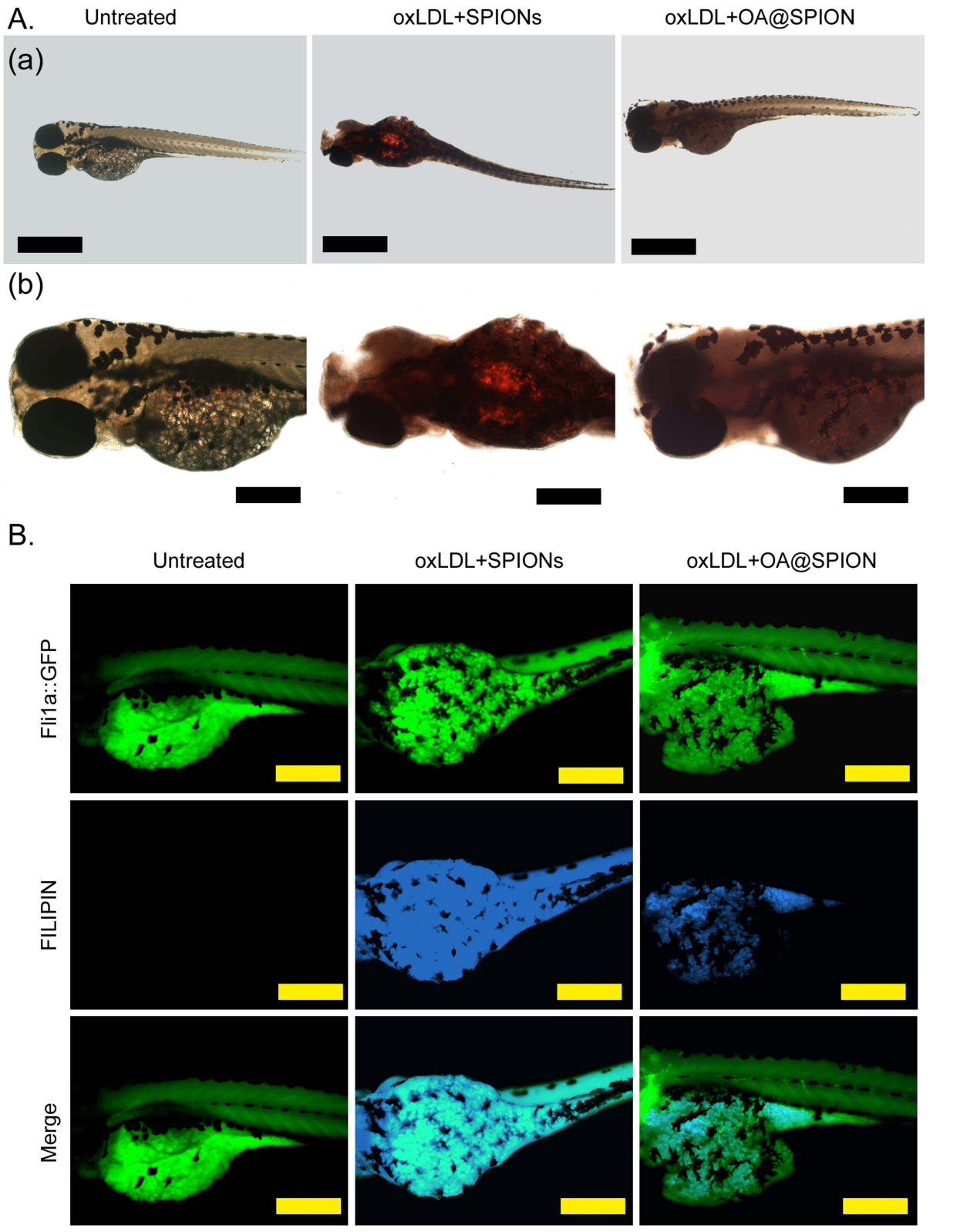

Figure 4 Pathological staining shows that OA@SPION-PEI alleviates oxLDL-induced lipid deposition in zebrafish organs. (**A**) Oil Red O staining of zebrafish in the OA@SPION-PEI group exhibited a light red coloration, indicating significant improvement in lipid deposition. (a) Magnification: 40×. Scale bar: 500 μm. (b) Magnification: 100×. Scale bar: 200 μm. (**B**) Filipin staining of the OA@SPION-PEI group showed significantly reduced lipid deposition in various zebrafish organs. Magnification: 100×. Scale bar: 200 μm.

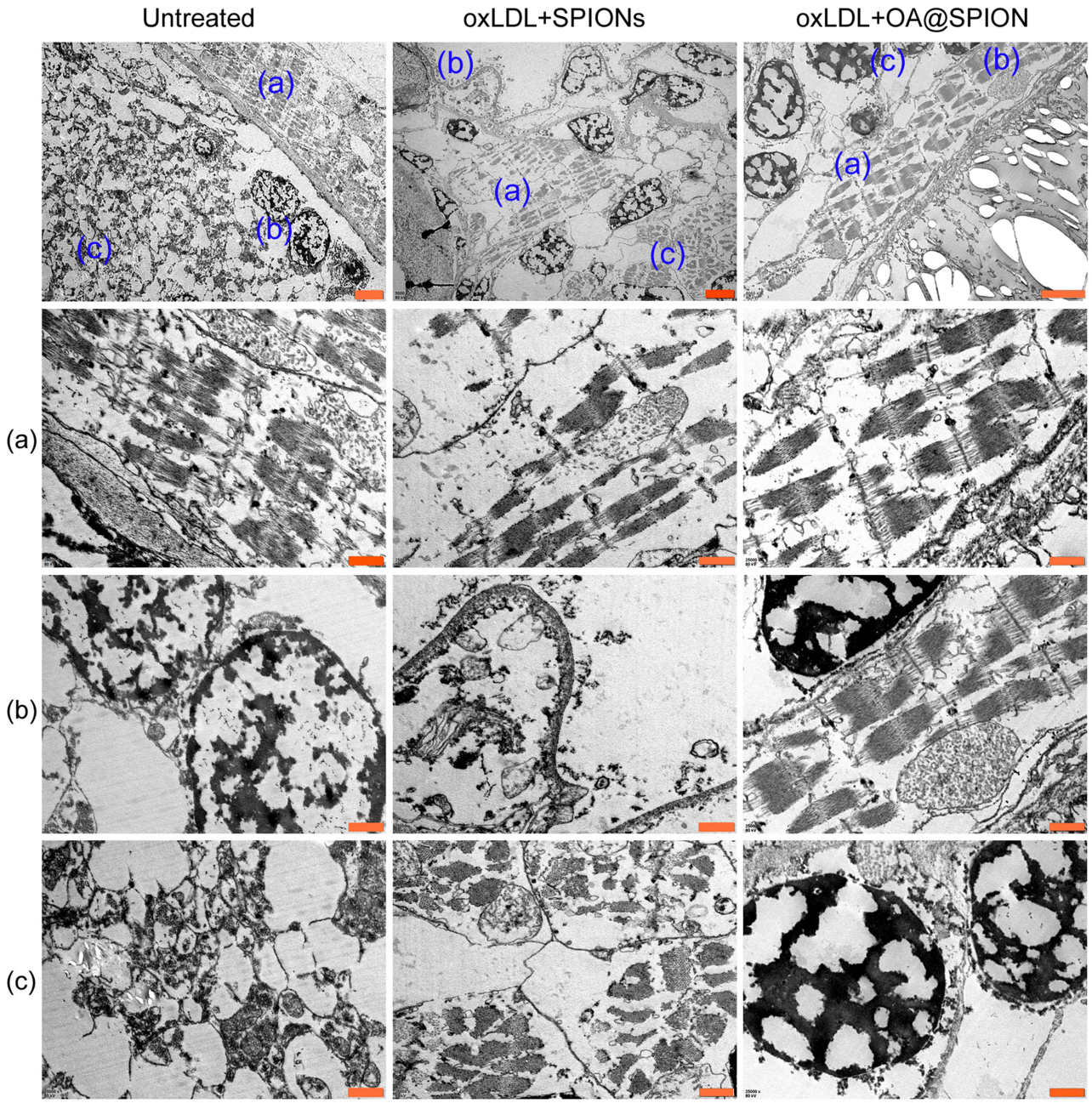

Figure 5 Transmission electron microscopy confirms protective effects of OA@SPION-PEI on microstructure of zebrafish tissues and organs. (**a**) OA@SPION-PEI group showed significant restoration of cardiomyocyte structure. Scale bar = 2 μm. (**b**) OA@SPION-PEI group showed significant restoration of intestinal cell structure. Scale bar = 2 μm. (**c**) OA@SPION-PEI group showed significant restoration of liver cell structure. Scale bar = 2 μm.

oxLDL+SPIONs groups, the differentially expressed gene transcripts were primarily related to signaling pathways such as galactose metabolism (Figure 6G and Supplementary Data Figure S5). These research findings suggest that oxLDL can alter the expression levels of multiple gene transcripts in zeECs.

OA@SPION-PEI Treatment Alters Gene Transcript Expression Levels in zeECs in an Atherosclerosis Model

To determine the effect of OA@SPION on gene transcripts in oxLDL-induced zebrafish atherosclerosis model zeECs, we conducted four comparisons of the intersections of transcripts from two groups: the oxLDL+SPIONs group vs the

https://doi.org/10.2147/DDDT.S512752

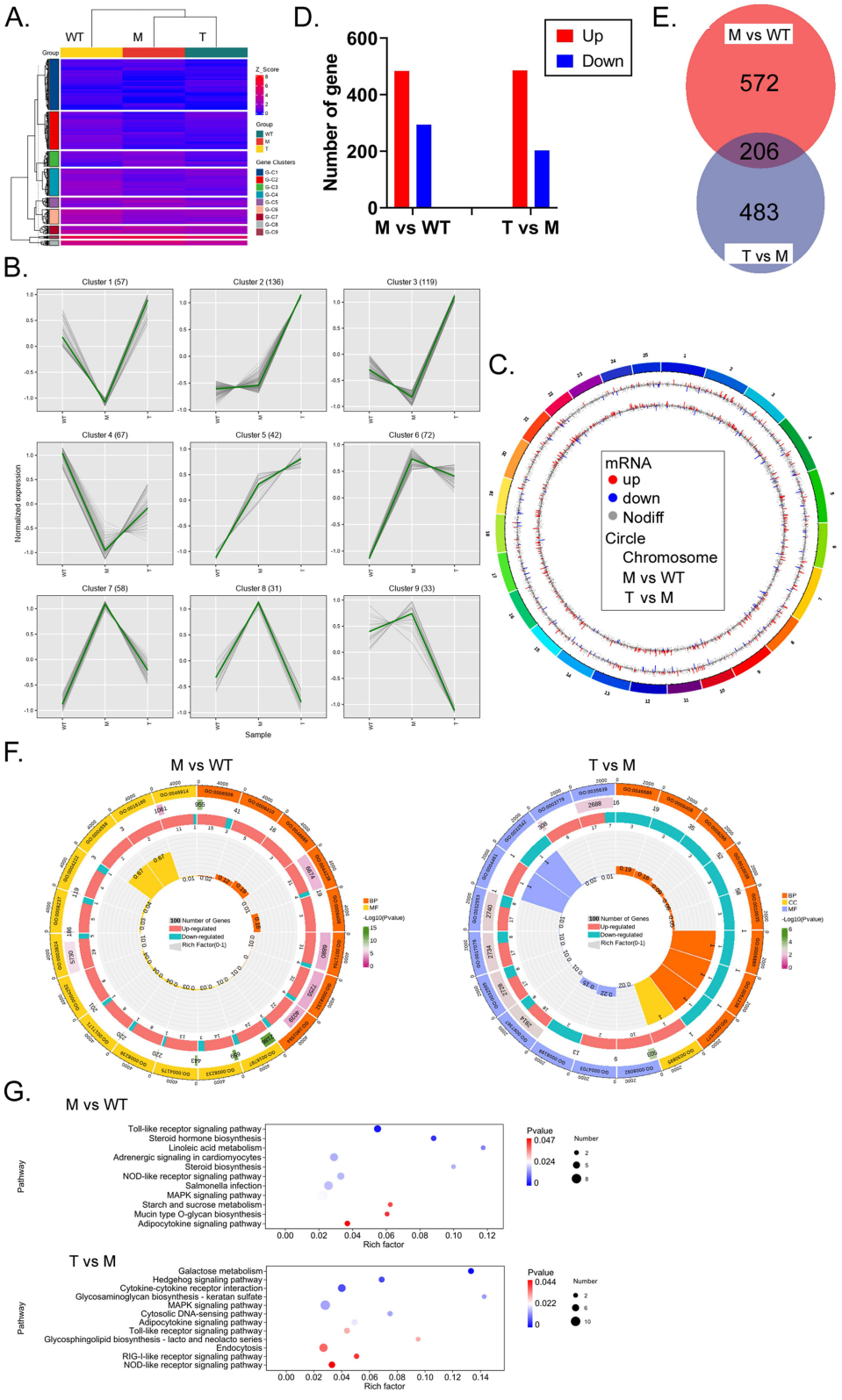

Figure 6 oxLDL alters expression levels of multiple gene transcripts in zeECs. (**A**) Heatmap showed the patterns of gene transcript level changes detected by RNA-seq in various groups. (**B**) Differential expression characteristics of gene sets acrossed nine clusters in different samples. (**C**) Locations and differential expression peaks of all gene transcripts mapped to 25 chromosomes. (**D**) Statistical analysis of upregulated and downregulated gene transcripts between the oxLDL+SPIONs group (M) and the untreated group (WT) and between the oxLDL+OA@SPION-treated group (T) and the oxLDL+SPIONs group (M). (**E**) Intersection results of differential transcripts among the three sample groups. (**F**) GO analysis predictions for the functions of differential gene transcripts among the three sample groups. (**G**) KEGG analysis predictions for the functions of differential gene transcripts among the three sample groups.

untreated group (high), the oxLDL+OA@SPION-treated group vs the oxLDL+SPIONs group (low; group 1), the oxLDL +SPIONs group vs the untreated group (low), and the oxLDL+OA@SPION-treated group vs the oxLDL+SPIONs group (high; group 2; Figure 7A). The statistical analysis indicated that group 1 included 64 differentially expressed transcripts, which represented transcripts significantly downregulated after OA@SPION treatment (Figure 7A, B and Supplementary Data Figure S6). Conversely, group 2 included 142 differentially expressed transcripts representing transcripts significantly upregulated after OA@SPION treatment (Figure 7A, B and Supplementary Data Figure S6). GO analysis revealed that the significantly downregulated transcripts in group 1 were associated with BPs such as response to cadmium ion, CCs such as the lipopolysaccharide receptor complex, and MFs such as cholesterol 25-hydroxylase activity (Figure 7C and Supplementary Data Figure S7). On the other hand, the significantly upregulated transcripts in group 2 were linked to BPs such as germ cell development, integral components of the membrane (CCs), and mitogen-activated protein (MAP) kinase activity (MF; Figure 7C and Supplementary Data Figure S7). Additionally, KEGG analysis demonstrated that the significantly downregulated transcripts in group 1 were primarily associated with signaling pathways such as the mitogen-activated protein kinase (MAPK) signaling pathway (Figure 7D and Supplementary Data Figure S8). In contrast, the significantly upregulated transcripts in group 2 were involved in signaling pathways such as gap junctions (Figure 7D and Supplementary Data Figure S8). Overall, these findings suggest that after oxLDL+SPION treatment, the expression levels of multiple gene transcripts and the associated physiological and biochemical signaling pathways in zeECs of the zebrafish atherosclerosis model undergo significant changes with OA@SPION treatment.

OA@SPION-PEI Mitigates oxLDL-Induced Damage to zeECs by Regulating JNK and MAPK Signaling Pathway Expression

Integration of the RNA-seq and KEGG prediction results indicates that OA@SPION has a role in modulating the expression of the JNK and MAPK signaling pathways, which are positively correlated with inflammation activation and cell apoptosis (Figure 8A). Heatmap and visualization analyses revealed that in the OA@SPION-treated group, the key genes involved in the JNK and MAPK signaling pathways, such as Cacna1c, Rab1ab (Ras), Map3k1 (MEKK1), Mapk8b (JNK), and JunD showed significantly lower sequencing signals compared with the oxLDL +SPION-treated group (Figure 8B and C). The qPCR results further indicated that the mRNA expression levels of Cacna1c, Rab1ab, Map3k1, Mapk8b, and JunD were significantly lower in the OA@SPION-treated group zeECs compared with the control group zeECs, whereas the expression levels of the negatively regulated genes HSP70.1 and HSP70.3 exhibited an opposite trend (Figure 8D). Therefore, the experimental findings suggest that OA@SPION likely alleviates oxLDL-induced damage to zeECs by regulating the expression of the JNK and MAPK signaling pathways.

Discussion

The aging of vascular ECs, lipid deposition, and inflammatory cell infiltration collectively exacerbate the occurrence and development of atherosclerosis.[1–3,35] Atherosclerosis significantly impacts human health and longevity, making the search for effective therapeutic agents essential. Recent reports indicate that OA exerts various beneficial effects, including the reduction of reactive oxygen species (ROS), the accumulation of lipid peroxides, and the mitigation of chronic inflammation.[15–17,19,33] However, OA also has critical drawbacks, such as poor water solubility and low cellular absorption and bioavailability, which severely hinder its therapeutic efficacy.[15–17] Currently, nanomedicine is gaining traction among clinical drug developers due to its high loading capacity, excellent cell membrane permeability, low toxicity, and stable sustained-release capabilities.[21–23,25]

Increasing evidence supports that SPIONs can effectively combine with various lipophilic or hydrophilic drugs to facilitate their efficient delivery into cells.[21–23,25] In light of this evidence, we aimed to load OA onto the surface of SPIONs to create an OA@SPION-PEI nanomedicine and explore its therapeutic effects and target mechanisms in a zebrafish model of atherosclerosis. We selected zebrafish as a novel model organism for studying lipid metabolism because it has several advantages over mice.[35–37] First, high-cholesterol diets can induce early phenotypes of hypercholesterolemia and atherosclerosis in zebrafish without requiring genetic mutations.[35–37] Additionally, zebrafish larvae can

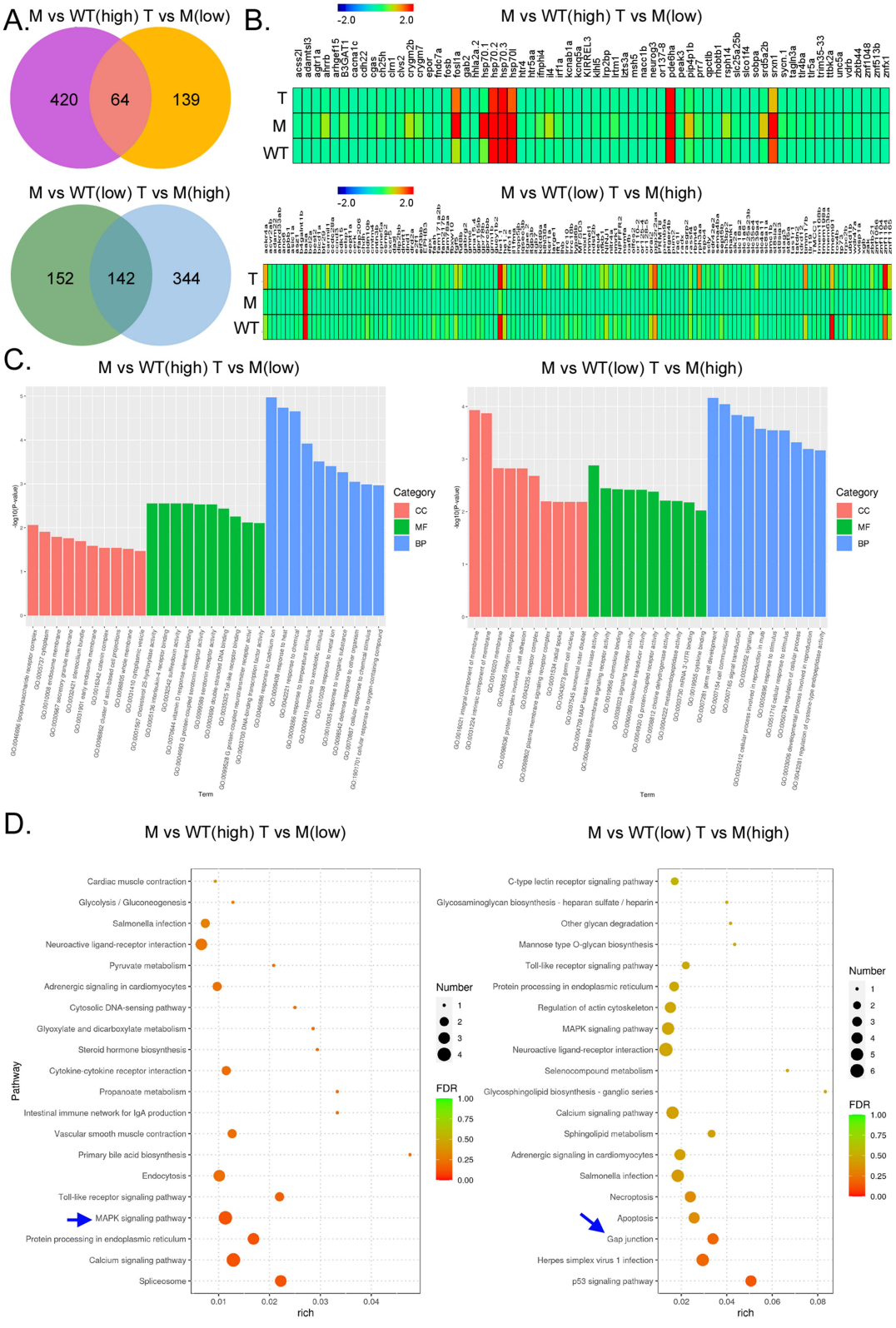

Figure 7 OA@SPION-PEI alters expression levels of multiple gene transcripts in zeECs. (**A**) Intersection results of significantly differentially expressed gene transcripts obtained from pairwise comparisons among the three sample groups. (**B**) Heatmap results of significantly differentially expressed gene transcripts obtained from pairwise comparisons among the three sample groups. (**C**) GO analysis predictions for significantly differentially expressed gene transcripts obtained from pairwise comparisons among the three sample groups. (**D**) KEGG analysis predictions for significantly differentially expressed gene transcripts obtained from pairwise comparisons among the three sample groups.

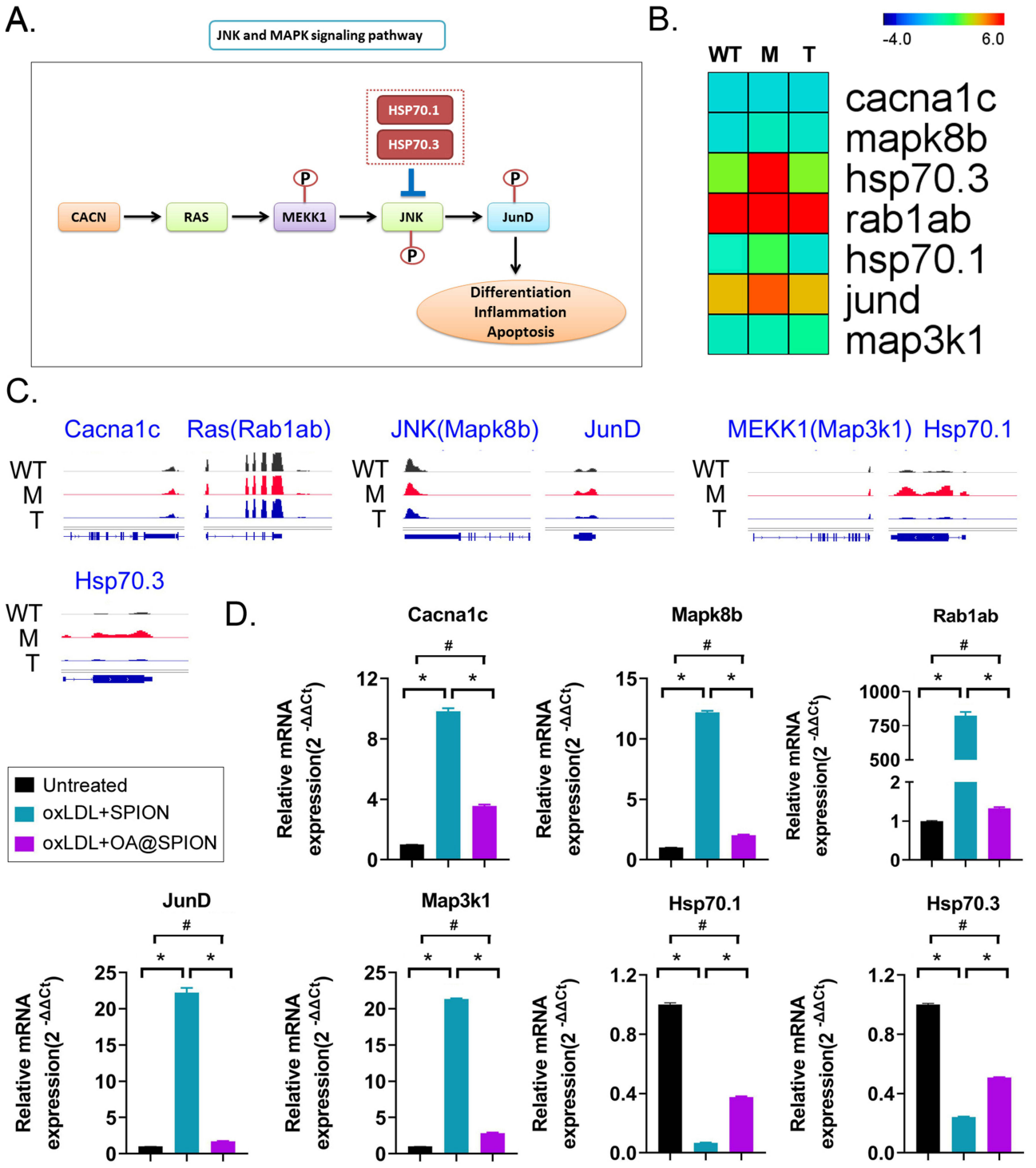

Figure 8 OA@SPION-PEI alleviates oxLDL-induced damage to zeECs by regulating expression of JNK and MAPK signaling pathways. (**A**) Composition of the JNK and MAPK signaling pathways. (**B**) Heatmap showing that OA@SPION-PEI significantly reduced the transcript levels of key genes in the JNK and MAPK signaling pathways in zeECs. (**C**) Visualization results indicated that OA@SPION-PEI significantly reduced the transcript levels of key genes in the JNK and MAPK signaling pathways in zeECs. (**D**) qPCR results indicated that the mRNA expression levels of genes such as Cacna1c, Rab1ab, Map3k1, Mapk8b, and JunD are significantly decreased in the OA@SPION-PEI-treated group zeECs. #p<0.01, One-Way ANOVA using Bonferroni test; *p<0.01, *t* test.

remain transparent for nearly a month after drug treatment, facilitating live imaging observations. Zebrafish also have short breeding cycles, high fecundity, and low maintenance costs.[35–37] Considering the crucial role of ECs in the pathogenesis of atherosclerosis, we utilized a specialized transgenic zebrafish (fli1a::EGFP+ zeECs) that labels ECs

https://doi.org/10.2147/DDDT.S512752

with GFP. This approach permits precise isolation of vascular ECs and subsequent gene sequencing analysis, allowing us to accurately explore the impact of OA@SPION-PEI on zeEC gene expression.

Through systematic pathological examination, oxidized low-density lipoprotein (oxLDL) has been confirmed to significantly induce lipid deposition, cellular aging, and structural damage in multiple organs of zebrafish. In contrast, OA@SPION-PEI has been observed to significantly alleviate these pathological injuries. By isolating and enriching Fli1a::EGFP+ zeECs from various groups and performing high-throughput RNA-seq, we found that OA@SPION-PEI can significantly improve the gene expression levels in a substantial group of ECs, with expression trends similar to those observed in untreated ECs. The high-throughput sequencing results indicate that OA@SPION-PEI may alleviate the pathological damage caused by oxLDL by correcting the expression levels of multiple genes. Furthermore, bioinformatics predictions combined with the molecular biology experiments suggest that OA@SPION-PEI likely mitigates oxLDL-induced damage to zeECs by regulating the expression of the JNK and MAPK signaling pathways.

An increasing number of studies have reported that the activation of the JNK and MAPK signaling pathways is positively correlated with cellular inflammation, apoptosis, differentiation, and injury.[38,39] Several studies have pointed out that effectively inhibiting the activity of the JNK and MAPK signaling pathways can significantly improve the pathological manifestations of atherosclerosis. Zhang et al confirmed that Astragaloside IV inhibited inflammation to attenuate atherosclerosis and hepatic steatosis by decreasing the phosphorylation levels of JNK, ERK1/2, p38, and NF-κB in the MAPK/NF-κB signaling pathway in LDLR-/- mice.[40] Geng et al found that the MAPK and JNK inhibitors could reduce the expression of the CD36/MAPK/JNK pathway and the formation of foam cells and atherosclerosis induced by ox-LDL and trimethylamine N-oxide.[41] Zhao et al reported that IL-4 may induce macrophages to take on an M2 phenotype to attenuate inflammation via inhibition of MAPK signaling pathway activity, including expression of p-ERK and p-JNK, thereby protecting against atherosclerosis.[42]

Several environmental toxicology studies have shown that di-N-butyl-phthalate increases the levels of phosphorylation modifications of p-ERK1/2 and p-JNK in the JNK and ERK1/2 MAPK signaling pathways, leading to increased testicular damage in rats.[43] Furthermore, microplastics have been found to induce murine reproductive toxicity through oxidative stress and activation of the p38 MAPK signaling pathways.[44] These findings demonstrate that activation of the JNK and MAPK signaling pathways significantly increases inflammation release and oxidative stress damage and exacerbates the pathological damage of atherosclerosis. Our findings are consistent with these reports, further validating the reliability of our experimental data. We also confirmed that OA@SPION-PEI is likely to alleviate oxLDL-induced damage to zebrafish zeECs by downregulating the expression of the JNK and MAPK signaling pathways.

In addition, both RNA high-throughput sequencing results and pathological staining results confirmed that OA@SPION-PEI could significantly improve the symptoms of atherosclerosis in zebrafish. Meanwhile, OA@SPION-PEI also significantly inhibited the expression of JNK and MAPK signaling pathway. And, the KEGG prediction results also indicated that the expression level differences of the gene cluster involved in the above signal transduction pathways were the most significant. Therefore, we have reason to believed that OA@SPION-PEI improved lipid-oxidative stress injury of zebrafish vessels via alleviating the JNK and MAPK signaling pathways in endothelial cells. After in-depth analysis of JNK and MAPK signaling pathway, we found that there is a negative regulatory factor on this pathway, namely HSP70.1 and HSP70.3, members of the heat shock protein family. They achieve negative regulation of the entire pathway by negatively regulating the expression of JNK protein. Our qPCR results showed that the expression levels of HSP70.1 and HSP70.3 were significantly higher in the samples of OA@SPION-PEI treated group than them in the control group. The result indicated the regulatory targets of OA@SPION-PEI for the JNK and MAPK signaling pathways are likely to be HSP70.1 and HSP70.3. We speculated that OA@SPION-PEI may negatively regulated the expression of JNK protein by activating the expression of HSP70.1 and HSP70.3 in vascular endothelial cells, thereby achieving inhibitory effects on the JNK and MAPK signaling pathways. Of course, due to limitations in time and funding, further research was not conducted. However, we believe that above result is very exciting. Meanwhile, in our subsequent study, we will in-depth explore the molecular biology mechanisms underlying the interaction between OA@SPION-PEI and of HSP70.1, HSP70.3.

In this study, we did not evaluate the long-term toxicity of SPIONs on zebrafish. We have referred to many clinical research reports in the past 20 years and found that multiple SPIONs derived contrast agents were used for clinical

diagnosis, and have fully demonstrated their safety and reliability in humans. To date, multiple companies and enterprises around the world have participated in the research and development of SPIONs contrast agents, and various commercial products have been launched.[25,45–48] For example, the Advanced Magnetics Company (Cambridge, MA, USA) was the first to launch the drug GastroMark (Ferumoxsil) based on magnetic iron oxide nanomaterials, based on a large amount of clinical data, and was approved for clinical diagnosis in Europe in 1993.[25,45–48] In 1996, the US Food and Drug Administration (FDA) approved Advanced Magnetics Company intravenous formulation Feridex for hepatic imaging.[25,45–48] In 2000, the Resovist (Ferucarbotran) developed by Schering (BAYER Group) for liver imaging was officially approved for clinical use in Europe. Subsequently, the lymphatic system contrast agent Combidex (Sinerem) has been appeared.[25,45–48] At present, more than 10 clinical products have been developed based on magnetic nanoparticles.[25,45–48] In addition, Ferumoxytol, consists of an iron oxide core nanoparticle coated with carboxymethyl-dextran, which has been primarily used as an iron injection for anemia. It provides an alternative approach for MRI of atherosclerotic plaques. Ferumoxytol can be taken up by macrophages in the atherosclerosis plaque and provide localized signal and imaging. For instance, In 2016, Semple et al applied Ferumoxytol for MR T2-weighted imaging with the potential application towards atherosclerosis.[49,50] Numerous clinical trials have confirmed that these magnetic nanoparticles derived contrast agents are safe for the human body.[25,45–48]

Our study confirms that SPIONs can effectively deliver OA for stable release in zebrafish and provides strong evidence that OA@SPION-PEI protects against oxLDL damage in zebrafish by lowering the expression levels of the JNK and MAPK signaling pathways (Figure 9).

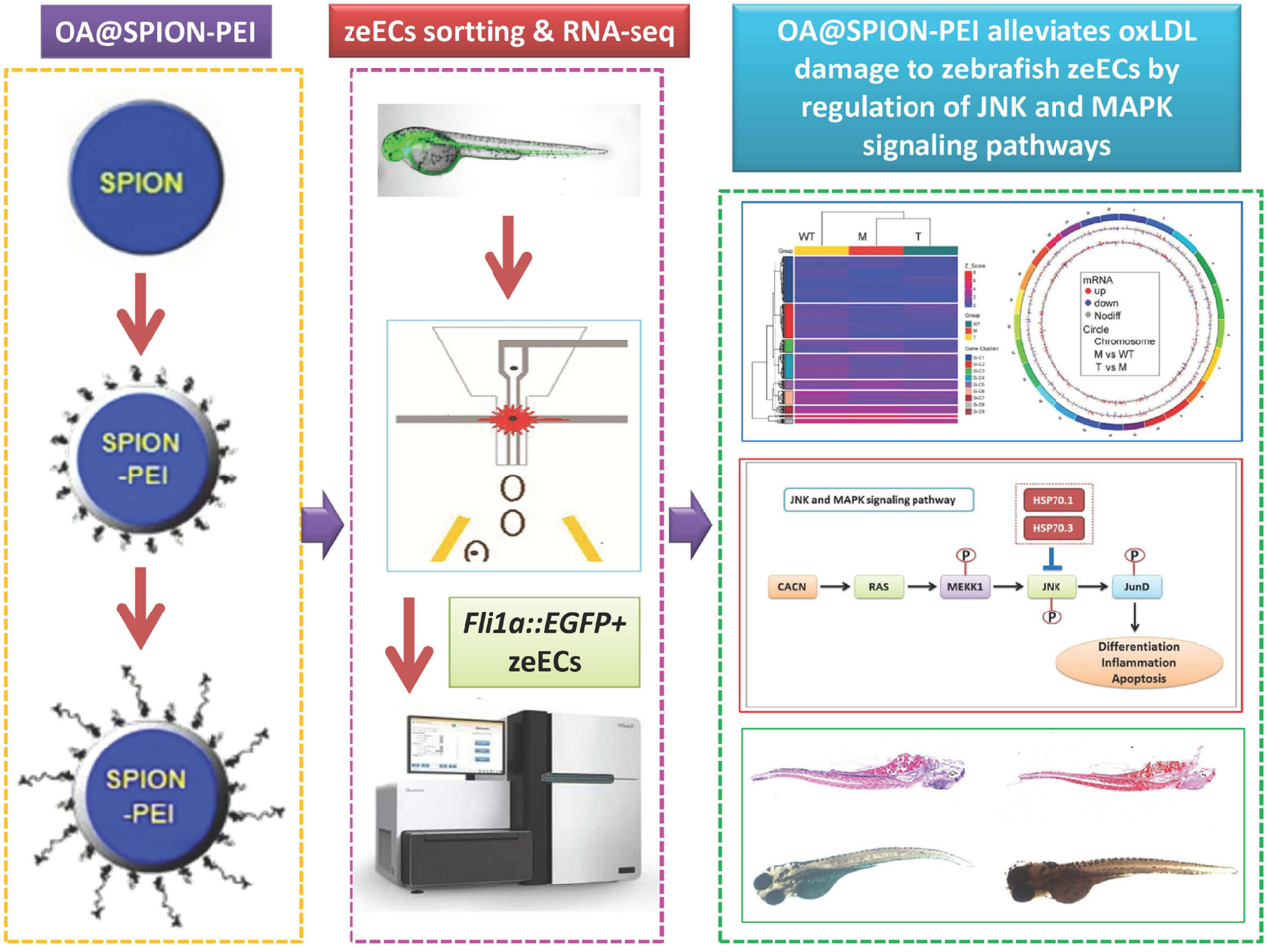

Figure 9 OA@SPION-PEI protects against lipid damage in zebrafish by lowering expression levels of JNK and MAPK signaling pathways.

https://doi.org/10.2147/DDDT.S512752

Data Sharing Statement

The datasets used or analysed during the current study are available from the corresponding author on reasonable request.

Acknowledgments

We thank LetPub (www.letpub.com) for its linguistic assistance during the preparation of this manuscript. Hongguo Gao, Te Liu, Junfeng Liu, Lian Yang, and Luxi Liu shared the first authorship.

Author Contributions

All authors made a significant contribution to the work reported, whether that is in the conception, study design, execution, acquisition of data, analysis and interpretation, or in all these areas; Te Liu, Yun Gu, Peirong Huang took part in drafting, revising or critically reviewing the article; all other authors took part in revising the article; all authors gave final approval of the version to be published; have agreed on the journal to which the article has been submitted; and agree to be accountable for all aspects of the work.

Funding

This work was supported by Shanghai Pujiang Program (22PJ1412100) and National Natural Science Foundation of China (82371073).

Disclosure

The authors declare that they have no conflicts of interest.

References

1. Libby P. The changing landscape of atherosclerosis. *Nature*. 2021;592(7855):524–533. doi:10.1038/s41586-021-03392-8
2. Kobiyama K, Ley K. Atherosclerosis. *Circ Res*. 2018;123(10):1118–1120. doi:10.1161/CIRCRESAHA.118.313816
3. Gimbrone Jr MA, Garcia-Cardena G. Endothelial Cell Dysfunction and the Pathobiology of Atherosclerosis. *Circ Res*. 2016;118(4):620–636. doi:10.1161/CIRCRESAHA.115.306301
4. Wang W, Li H, Shi Y, et al. Targeted intervention of natural medicinal active ingredients and traditional Chinese medicine on epigenetic modification: possible strategies for prevention and treatment of atherosclerosis. *Phytomedicine*. 2024;122:155139. doi:10.1016/j.phymed.2023.155139
5. Zhai KF, Duan H, Shi Y, et al. miRNAs from Plasma Extracellular Vesicles Are Signatory Noninvasive Prognostic Biomarkers against Atherosclerosis in LDLr(-/-)Mice. *Oxid Med Cell Longev*. 2022;2022:6887192. doi:10.1155/2022/6887192
6. Duan H, Li H, Liu T, et al. Exploring the Molecular Mechanism of Schisandrin C for the Treatment of Atherosclerosis via the PI3K/AKT/mTOR Autophagy Pathway. *ACS omega*. 2024;9(30):32920–32930. doi:10.1021/acsomega.4c03738
7. Zhai K, Deng L, Wu Y, et al. Extracellular vesicle-derived miR-146a as a novel crosstalk mechanism for high-fat induced atherosclerosis by targeting SMAD4. *J Adv Res*. 2024. doi:10.1016/j.jare.2024.08.012
8. American Association of Neurological Surgeons, Interventional Radiology Society of Europe, CIRACoNSESoMINTESoNESOSfCA, Interventions, SoIRSoNS, Sacks D, Baxter B, Campbell BCV, et al. Multisociety Consensus Quality Improvement Revised Consensus Statement for Endovascular Therapy of Acute Ischemic Stroke. *Int J Stroke*. 2018;13(6):612–632. doi:10.1177/1747493018778713.
9. Kruger-Genge A, Blocki A, Franke RP, et al. Vascular Endothelial Cell Biology: an Update. *Int J mol Sci*. 2019;20(18):4411. doi:10.3390/ijms20184411
10. Breitling J, Aebi M. N-linked protein glycosylation in the endoplasmic reticulum. *Cold Spring Harb Perspect Biol*. 2013;5(8):a013359. doi:10.1101/cshperspect.a013359
11. Zhou AX, Tabas I. The UPR in atherosclerosis. *Semin Immunopathol*. 2013;35(3):321–332. doi:10.1007/s00281-013-0372-x
12. Dookun E, Walaszczyk A, Redgrave R, et al. Clearance of senescent cells during cardiac ischemia–reperfusion injury improves recovery. *Aging Cell*. 2020;19(10):e13249. doi:10.1111/acel.13249
13. Anderson R, Lagnado A, Maggiorani D, et al. Length-independent telomere damage drives post-mitotic cardiomyocyte senescence. *EMBO J*. 2019;38(5). doi:10.15252/embj.2018100492.
14. Childs BG, Baker DJ, Wijshake T, et al. Senescent intimal foam cells are deleterious at all stages of atherosclerosis. *Science*. 2016;354(6311):472–477. doi:10.1126/science.aaf6659
15. Castellano JM, Ramos-Romero S, Perona JS. Oleanolic Acid: extraction, Characterization and Biological Activity. *Nutrients*. 2022;14(3):623. doi:10.3390/nu14030623
16. Pollier J, Goossens A. Oleanolic acid. *Phytochemistry*. 2012;77:10–15. doi:10.1016/j.phytochem.2011.12.022
17. Ayeleso TB, Matumba MG, Mukwevho E. Oleanolic Acid and Its Derivatives: biological Activities and Therapeutic Potential in Chronic Diseases. *Molecules*. 2017;22(11):1915. doi:10.3390/molecules22111915
18. Liu T, Wang J, Tong Y, et al. Integrating network pharmacology and animal experimental validation to investigate the action mechanism of oleanolic acid in obesity. *J Transl Med*. 2024;22(1):86. doi:10.1186/s12967-023-04840-x

19. Sureda A, Monserrat-Mesquida M, Pinya S, et al. Hypotensive Effects of the Triterpene Oleanolic Acid for Cardiovascular Prevention. *Curr Mol Pharmacol*. 2021;14(6):935–942. doi:10.2174/1874467213999201230211544
20. Luo Q, Wei Y, Lv X, et al. The Effect and Mechanism of Oleanolic Acid in the Treatment of Metabolic Syndrome and Related Cardiovascular Diseases. *Molecules*. 2024;29:1.
21. Unalan I, Occhipinti I, Miola M, et al. Development of Super-Paramagnetic Iron Oxide Nanoparticle-Coated Melt Electrowritten Scaffolds for Biomedical Applications. *Macromol Biosci*. 2024;24(3):e2300397. doi:10.1002/mabi.202300397
22. Khan SA, Sharma R. Super Para-Magnetic Iron Oxide Nanoparticles (SPIONs) in the Treatment of Cancer: challenges, Approaches, and its Pivotal Role in Pancreatic, Colon, and Prostate Cancer. *Curr Drug Deliv*. 2023;20(6):643–655. doi:10.2174/1567201819666220509164611
23. Talluri S, Malla RR. Superparamagnetic Iron Oxide Nanoparticles (SPIONs) for Diagnosis and Treatment of Breast, Ovarian and Cervical Cancers. *Curr Drug Metab*. 2019;20(12):942–945. doi:10.2174/1389200220666191016124958
24. Hossen S, Hossain MK, Basher MK, et al. Smart nanocarrier-based drug delivery systems for cancer therapy and toxicity studies: a review. *J Adv Res*. 2019;15:1–18. doi:10.1016/j.jare.2018.06.005
25. Bakhtiary Z, Saei AA, Hajipour MJ, et al. Targeted superparamagnetic iron oxide nanoparticles for early detection of cancer: possibilities and challenges. *Nanomedicine*. 2016;12(2):287–307. doi:10.1016/j.nano.2015.10.019
26. Shokrollahi H. Contrast agents for MRI. *Mater Sci Eng C Mater Biol Appl*. 2013;33(8):4485–4497. doi:10.1016/j.msec.2013.07.012
27. Krueger J, Liu D, Scholz K, et al. Flt1 acts as a negative regulator of tip cell formation and branching morphogenesis in the zebrafish embryo. *Development*. 2011;138(10):2111–2120. doi:10.1242/dev.063933
28. Ye W, Ni Z, Yicheng S, et al. Anisomycin inhibits angiogenesis in ovarian cancer by attenuating the molecular sponge effect of the lncRNA-Meg3/miR-421/PDGFRA axis. *Int J Oncol*. 2019;55(6):1296–1312. doi:10.3892/ijo.2019.4887
29. Li M, Hu D, Zhang D, et al. Encapsulation of oleanolic acid into cyclodextrin metal-organic frameworks by co-crystallization: preparation, structure characterization and its effect on a zebrafish larva NAFLD model. *Food Res Int*. 2025;204:115936. doi:10.1016/j.foodres.2025.115936
30. Soares ICR, Santos S, Coelho RF, et al. Oleanolic acid promotes orofacial antinociception in adult zebrafish (Danio rerio) through TRPV1 receptors. *Chem Biol Interact*. 2019;299:37–43. doi:10.1016/j.cbi.2018.11.018
31. Zhang H, Zheng J, Lin J, et al. miR-758 mediates oxLDL-dependent vascular endothelial cell damage by suppressing the succinate receptor SUCNR1. *Gene*. 2018;663:1–8. doi:10.1016/j.gene.2018.04.029
32. Guo J, Xiang Q, Xin Y, et al. miR-544 promotes maturity and antioxidation of stem cell-derived endothelial like cells by regulating the YY1/TET2 signalling axis. *Cell Commun Signal*. 2020;18(1):35. doi:10.1186/s12964-019-0504-6
33. Zhang B, Zhang W, Luo J, et al. Effects of oleanolic acid on hair growth in mouse dorsal skin mediated via regulation of inflammatory cytokines. *J Appl Biomed*. 2023;21(1):48–57. doi:10.32725/jab.2023.003
34. Stelling-Ferez J, Cappellacci I, Pandolfi A, et al. Oleanolic acid rescues critical features of umbilical vein endothelial cells permanently affected by hyperglycemia. *Front Endocrinol*. 2023;14:1308606. doi:10.3389/fendo.2023.1308606
35. Stoletov K, Fang L, Choi S-H, et al. Vascular lipid accumulation, lipoprotein oxidation, and macrophage lipid uptake in hypercholesterolemic zebrafish. *Circ Res*. 2009;104(8):952–960. doi:10.1161/CIRCRESAHA.108.189803
36. Tang D, Geng F, Yu C, et al. Recent Application of Zebrafish Models in Atherosclerosis Research. *Front Cell Dev Biol*. 2021;9:643697. doi:10.3389/fcell.2021.643697
37. Fang L, Harkewicz R, Hartvigsen K, et al. Oxidized cholesteryl esters and phospholipids in zebrafish larvae fed a high cholesterol diet: macrophage binding and activation. *J Biol Chem*. 2010;285(42):32343–32351. doi:10.1074/jbc.M110.137257
38. Zhang Z, Yang Z, Wang S, et al. Targeting MAPK-ERK/JNK pathway: a potential intervention mechanism of myocardial fibrosis in heart failure. *Biomed Pharmacother*. 2024;173:116413. doi:10.1016/j.biopha.2024.116413
39. Hammouda MB, Ford AE, Liu Y, et al. The JNK Signaling Pathway in Inflammatory Skin Disorders and Cancer. *Cells*. 2020;9(4):857. doi:10.3390/cells9040857
40. Zhang Y, Du M, Wang J, et al. Astragaloside IV Relieves Atherosclerosis and Hepatic Steatosis via MAPK/NF-κB Signaling Pathway in LDLR−/− Mice. *Front Pharmacol*. 2022;13:828161. doi:10.3389/fphar.2022.828161
41. Geng J, Yang C, Wang B, et al. Trimethylamine N-oxide promotes atherosclerosis via CD36-dependent MAPK/JNK pathway. *Biomed Pharmacother*. 2018;97:941–947. doi:10.1016/j.biopha.2017.11.016
42. Zhao XN, Li YN, Wang YT. Interleukin-4 regulates macrophage polarization via the MAPK signaling pathway to protect against atherosclerosis. *Genet Mol Res*. 2016;15(1). doi:10.4238/gmr.15017348
43. Wang H, Zhou W, Zhang J, et al. Role of JNK and ERK1/2 MAPK signaling pathway in testicular injury of rats induced by di-N-butyl-phthalate (DBP). *Biol Res*. 2019;52(1):41. doi:10.1186/s40659-019-0248-1
44. Xie X, Deng T, Duan J, et al. Exposure to polystyrene microplastics causes reproductive toxicity through oxidative stress and activation of the p38 MAPK signaling pathway. *Ecotoxicol Environ Saf*. 2020;190:110133. doi:10.1016/j.ecoenv.2019.110133
45. Weissleder R, Pittet MJ. Imaging in the era of molecular oncology. *Nature*. 2008;452(7187):580–589. doi:10.1038/nature06917
46. Sun C, Lee JSH, Zhang M. Magnetic nanoparticles in MR imaging and drug delivery. *Adv Drug Deliv Rev*. 2008;60(11):1252–1265. doi:10.1016/j.addr.2008.03.018
47. Corot C, Robert P, Idee JM, et al. Recent advances in iron oxide nanocrystal technology for medical imaging. *Adv Drug Deliv Rev*. 2006;58(14):1471–1504. doi:10.1016/j.addr.2006.09.013
48. Wagner V, Dullaart A, Bock AK, et al. The emerging nanomedicine landscape. *Nat Biotechnol*. 2006;24(10):1211–1217. doi:10.1038/nbt1006-1211
49. Nguyen KL, Yoshida T, Kathuria-Prakash N, et al. Multicenter Safety and Practice for Off-Label Diagnostic Use of Ferumoxytol in MRI. *Radiology*. 2019;293(3):554–564. doi:10.1148/radiol.2019190477
50. Chen J, Zhang X, Millican R, et al. Recent advances in nanomaterials for therapy and diagnosis for atherosclerosis. *Adv Drug Deliv Rev*. 2021;170:142–199. doi:10.1016/j.addr.2021.01.005